

FINITE ELEMENT ANALYSIS AND MODEL VALIDATION OF SHEAR DEFICIENT REINFORCED CONCRETE BEAMS STRENGTHENED WITH GFRP LAMINATES

Damian I. Kachlakev, Ph.D., P.E.
California Polytechnic State University

Abstract

An ANSYS finite element model is used to study the effects of shear strengthening by comparing the behaviors of two full-scale reinforced concrete beams (a reinforced concrete beam with no shear stirrups; and a reinforced concrete beam externally reinforced with Glass Fiber Reinforced Polymer (GFRP) on both sides of the beam). Experimental beams replicated the transverse members from the Horsetail Creek Bridge, which are deficient in shear reinforcement. Three-dimensional finite element models are developed using a smeared cracking approach for the concrete and three-dimensional layered elements for the FRP composites.

It was found that the general behaviors through the linear and nonlinear ranges up to failure of the finite element models show good agreement with observations and data from the experimental full-scale beam tests. The addition of GFRP reinforcement to the control beam shifts the behavior of the actual beam and model from a sudden shear failure near the ends of the beam to flexure failure by steel yielding at the midspan. The shear reinforcement increases the load carrying capacity by 45% for the experimental beam and by 15% for the finite element model. This finite element model can be used in additional studies to develop design rules for strengthening reinforced concrete bridge members using FRP.

KEY WORDS: Finite Element Analysis; Reinforced Concrete Beams; Fiber-Reinforced Polymers

Introduction

In the last decade, fiber reinforced polymer (FRP) composites have been used for strengthening structural members of reinforced concrete bridges, which are deficient or obsolete due to changes in their use or consideration of increased loadings. Many researchers have found that FRP composites applied to those members provide efficiency, reliability and cost effectiveness in rehabilitation ([10], [13], [18], [21]). Currently in the U.S., ACI Committee 440 is working to establish design recommendations for FRP application to reinforced concrete [2].

The Horsetail Creek Bridge was constructed in 1913. The bridge is in current use, located east of Portland, Oregon along the Historic Columbia River Highway, and is a historic structure. The transverse bridge beams were constructed without the presence of shear reinforcement [11]. External reinforcement with FRP composites was used to increase the strength of the beams due to the historic nature of the bridge, limited funding and time restrictions.

In this paper, the ANSYS finite element program [3] is used to simulate the behavior of two full-scale reinforced concrete beams, which replicated the transverse members from the Horsetail Creek Bridge [11]. The finite element model uses a smeared cracking approach and three-dimensional layered

elements to model FRP composites. This model can help to confirm the theoretical calculations as well as to provide a valuable supplement to the laboratory investigations of behavior.

Experimental Beams

Four full-scale reinforced concrete beams (similar to the transverse beams of the Horsetail Creek Bridge) were fabricated and tested at Oregon State University (a control beam, a shear-strengthened beam, a flexural-strengthened beam, and a beam with both shear and flexural strengthening) in order to compare their behaviors in the laboratory. Glass Fiber Reinforced Polymer (GFRP) was applied on the sides of the actual Horsetail Creek Bridge beams to provide increased shear strength, and Carbon Fiber Reinforced Polymer (CFRP) to the bottom of the beams to increase the flexural strength.

This paper focuses on the performance of the shear-strengthened beam; therefore the behaviors of the control reinforced concrete beam (no shear stirrups and no FRP reinforcement) and the shear-strengthened beam (added GFRP reinforcing on the sides) are compared. The experimental beams were tested in third point bending. Figure 2.1 illustrates these two experimental beams.

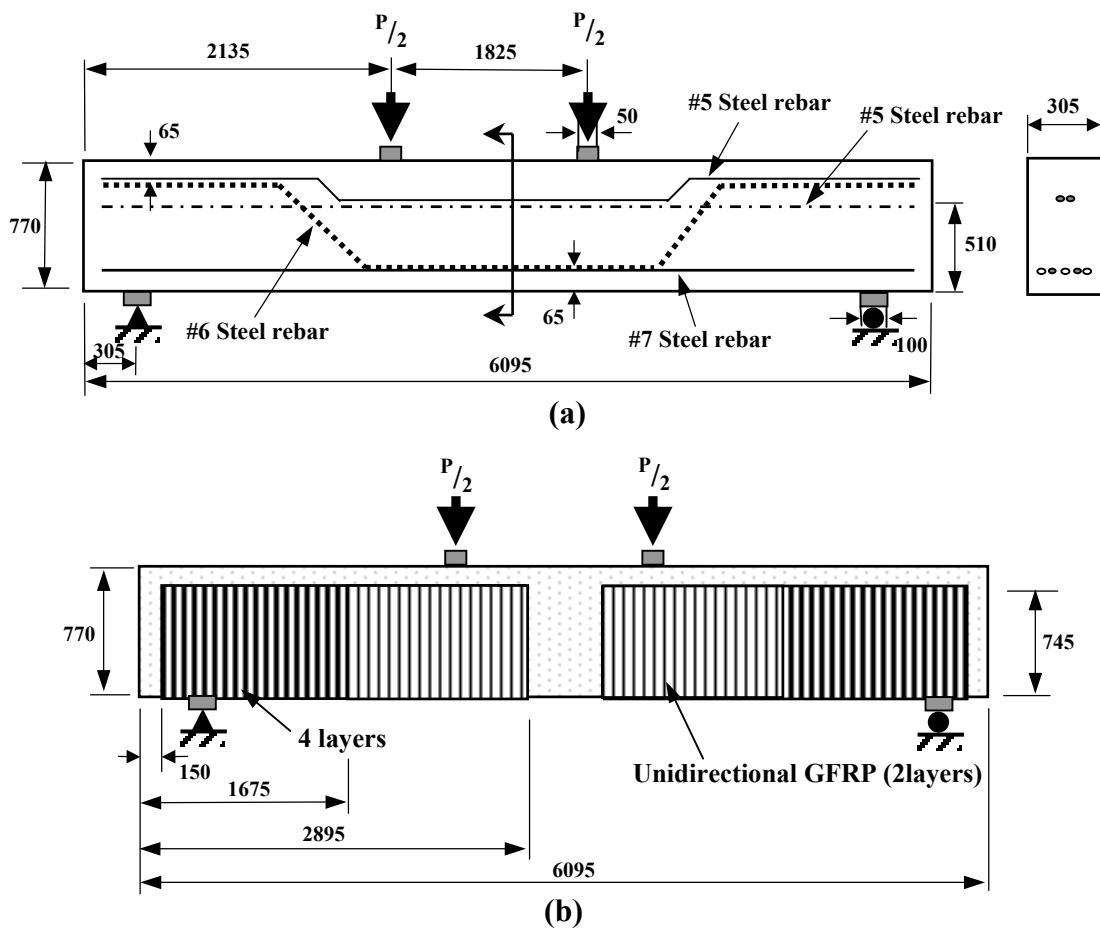


Figure 2.1: Experimental beams (dimensions shown in mm): (a) Control Beam; (b) Shear-Strengthened Beam [14]

Finite Element Models

Element Types

A solid element, SOLID65, is used to model the concrete in ANSYS. The solid element has eight nodes with three degrees of freedom at each node, translations in the nodal x, y, and z directions. The element is capable of plastic deformation, and cracking in three orthogonal directions. A LINK8 element is used to model the steel reinforcement. Two nodes are required for this element. At each node, degrees of freedom are identical to those for the SOLID65. The element is also capable of plastic deformation. A layered solid element, SOLID46, is used to model the GFRP composite. The element allows for up to 100 different material layers with different orientations, and orthotropic material properties in each layer. The element has three degrees of freedom at each node, translations in the nodal x, y, and z directions.

Material Properties

Concrete: SOLID65 elements are capable of predicting the nonlinear behavior of concrete materials using a smeared crack approach [22]. The smeared crack approach has been adopted widely in the recent decades ([16], [19], [4], [20]). Concrete is a quasi-brittle material and has very different behaviors in compression and tension. The tensile strength of concrete is typically 8-15% of the compressive strength. For the full-scale beam models, the elastic modulus for each beam was estimated using a pulse velocity method. The ultimate concrete compressive and tensile strengths for each beam model were calculated by Equations 1, and 2, respectively [1].

$$f'_c = \left(\frac{E_c}{4730} \right)^2 \quad (1)$$

$$f_r = 0.623(f'_c)^{\frac{1}{2}} \quad (2)$$

where:

E_c = elastic modulus of concrete, MPa

f'_c = ultimate compressive strength, MPa

f_r = ultimate tensile strength (modulus of rupture), MPa

Next, equations 3 and 4 [7] are used along with Equation 5 to construct the uniaxial compressive stress-strain curve for concrete in this study.

$$f = \frac{E_c \varepsilon}{1 + \left(\frac{\varepsilon}{\varepsilon_0} \right)^2} \quad (3)$$

$$\varepsilon_0 = \frac{2f'_c}{E_c} \quad (4)$$

$$E_c = \frac{f}{\varepsilon} \quad (5)$$

where:

f = stress at any strain ε , MPa

ε = strain at stress f

E_c = concrete elastic modulus, MPa

ε_0 = strain at the ultimate compressive strength f_c'

In tension, the stress-strain curve for concrete is assumed to be linearly elastic up to the ultimate tensile strength. After this point, the concrete cracks and the strength decreases to zero. Figure 3.1 shows the simplified uniaxial stress-strain relationship that is used in this study.

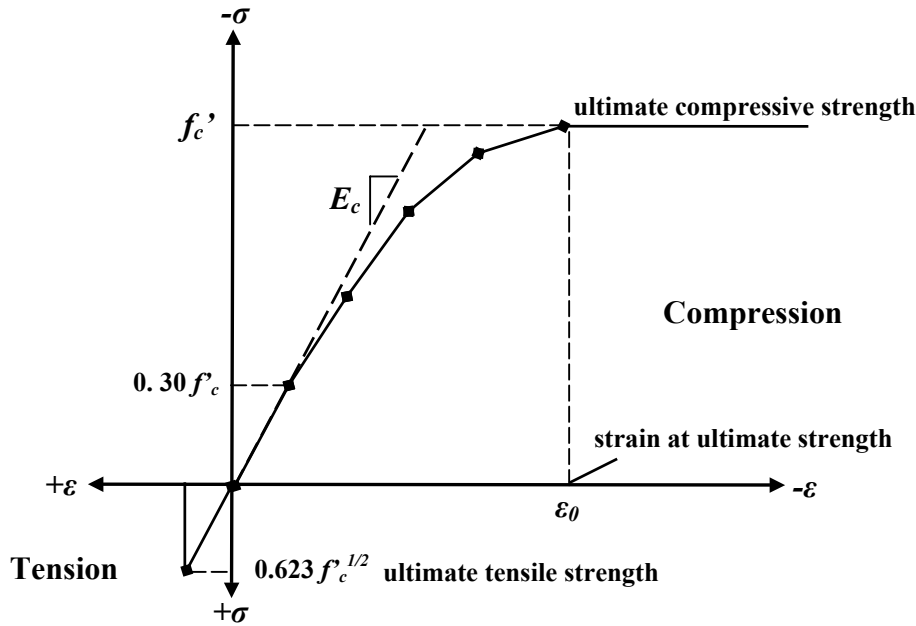


Figure 3.1: Simplified Uniaxial Stress-Strain Curve for Concrete

Poisson's ratio for concrete is assumed to be 0.2 and is used for all beams. The value of a shear transfer coefficient, representing conditions of the crack face, used in many studies of reinforced concrete structures varied between 0.05 and 0.25 ([5], [8], [9]). The shear transfer coefficient used in this study is equal to 0.2.

Steel Reinforcement and Steel Plates: Steel reinforcement in the experimental beams was constructed with typical steel reinforcing bars ($f_y = 415$ Mpa). Elastic modulus and yield stress for the steel reinforcement used in this FEM study follow the design material properties used for the experimental investigation. The steel for the finite element models is assumed to be an elastic-perfectly plastic material and identical in tension and compression. A Poisson's ratio of 0.3 is used for the steel reinforcement. Figure 3.2 shows the stress-strain relationship used in this study. Material properties for the concrete and steel reinforcement are summarized in Table 3.1.

For the finite element models, each load is distributed over a small area as for the experimental beams. A 25 mm thick steel plate, modeled using SOLID45 elements, is added at the support location in order to avoid stress concentration problems. This provides a more even stress distribution over the support area. An elastic modulus equal to 200 GPa and Poisson's ratio of 0.3 are used for the plates. The steel plates are assumed to be linear elastic materials.

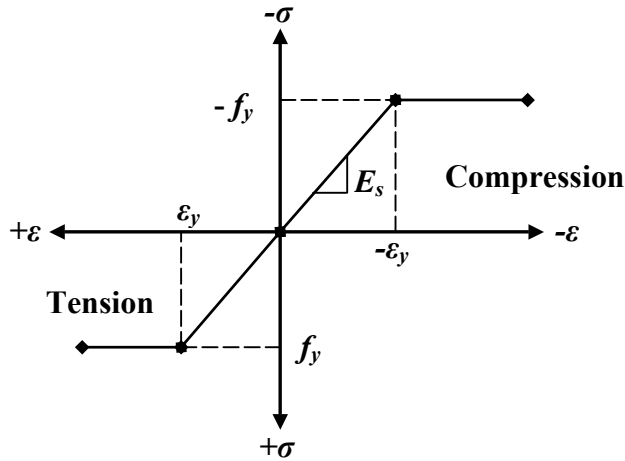


Figure 3.2: Stress-Strain Curve for Steel Reinforcement

Table 3.1: Summary of Material Properties for Reinforced Concrete

Beam	Concrete					Steel Rebar		
	E_c (GPa)	f_c' (MPa)	f_r (MPa)	ν	β_t	E_s (GPa)	f_y (MPa)	ν
Control beam	19.3	16.7	2.55	0.2	0.2	200	415	0.3
Shear beam	18.2	14.7	2.39	0.2	0.2	200	415	0.3

FRP Composites: For this study, the GFRP is assumed to be a specially orthotropic and transversely isotropic material, where the properties of the FRP composites are the same in any direction perpendicular to the fibers. GFRP is applied on the sides of the beams for increased shear strength, due to its superior strain at failure. Linear elastic properties of FRP composites are assumed throughout this study.

Table 3.2: Summary of Material Properties for GFRP Composite [11]

FRP composite	Elastic modulus (GPa)	Major Poisson's ratio	Tensile strength (MPa)	Shear modulus (GPa)	Thickness of laminate (mm)
GFRP	$E_x = 20.7$ $E_y = 6.89^*$ $E_z = 6.89^*$	$\nu_{xy} = 0.260$ $\nu_{xz} = 0.260$ $\nu_{yz} = 0.300^*$	600	$G_{xy} = 1.52$ $G_{xz} = 1.52$ $G_{yz} = 2.65^{**}$	1.3

*[10]

$$^{**} G_{yz} = \frac{E_{y \text{ or } z}}{2(1 + \nu_{yz})}$$

Modeling Methodology

By taking advantage of the symmetry of the beams, a quarter of the full beam is used for modeling with proper boundary conditions. This approach reduces computational time and computer disk space requirements significantly. The steel reinforcement is simplified in the model by ignoring the inclined portions of the steel bars present in the test beams. Ideally, the bond strength between the concrete and steel reinforcement should be considered. However, in this study, perfect bond between materials is assumed.

The various thickness of the FRP composites create discontinuities, which are not desirable for the finite element analysis. These may develop high stress concentrations at local areas on the models, yielding difficulties in convergence of the solutions. Therefore, a consistent thickness of FRP composites is used in the models to avoid discontinuities, by compensating with changes in the elastic and shear moduli in each layer. For example, if the thickness of FRP laminates is doubled, the elastic and shear moduli are both reduced by 50%. Note that the relationship between elastic and shear moduli is linear. Perfect bond between concrete and FRP laminates is assumed. A convergence study was carried out to determine an appropriate mesh density. Minor modification of dimensions for the FRP reinforcing was made due to geometric constraints from the other elements in the models, i.e. meshing of concrete elements, steel rebar locations and required output locations. Figure 3.3 shows the finite element models.

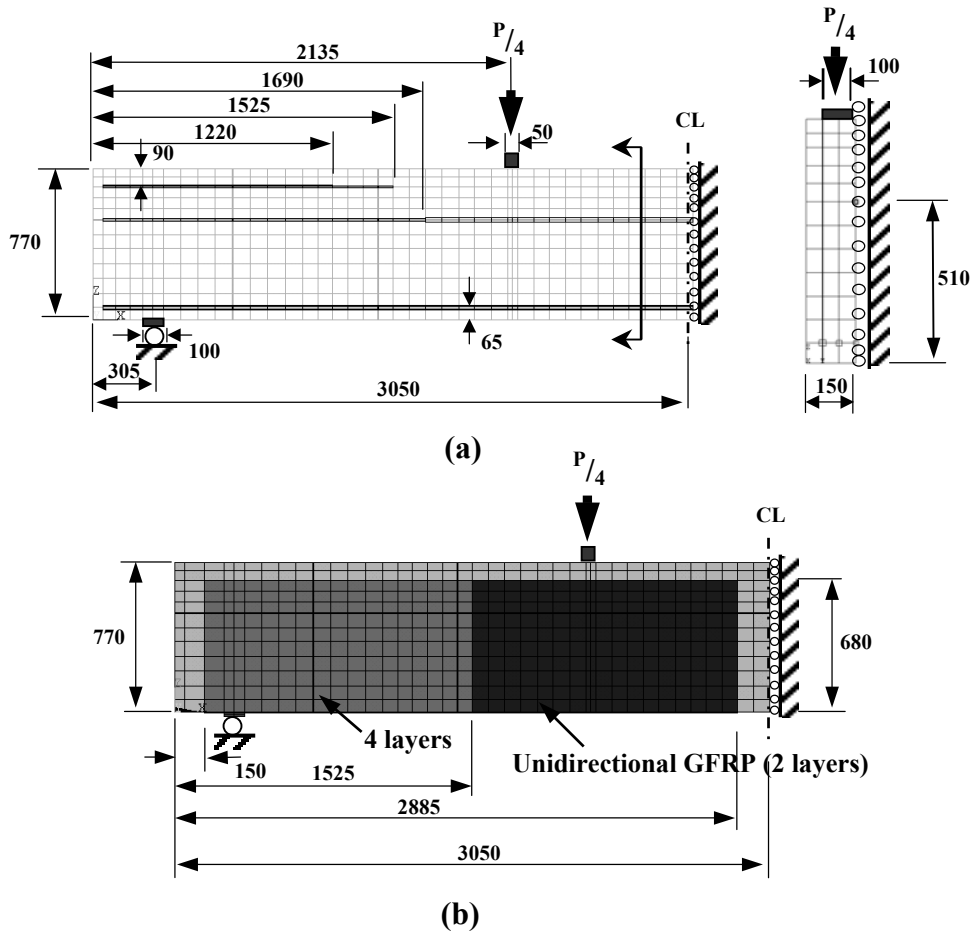


Figure 3.3: Finite Element Models (dimensions shown in mm): (a) Control Beam; (b) Shear-Strengthened Beam

Comparison of Results

Tensile Strain in Main Steel Reinforcing

Comparisons of the load-tensile strain plots from the finite element analyses and the experimental data for the main steel reinforcing at midspan are shown in Figure 4.1. For both the control and shear-strengthened beams in the linear range (before concrete cracking) the strains from the finite element analysis correlate well with those from the experimental data. In the nonlinear range, the trends of the finite element and the experimental results are generally similar. The finite element analysis supports the experimental results that the main steel rebar at midspan for the control beam has not yielded at failure, while the steel rebar for the shear-strengthened beam yields but at a lower load.

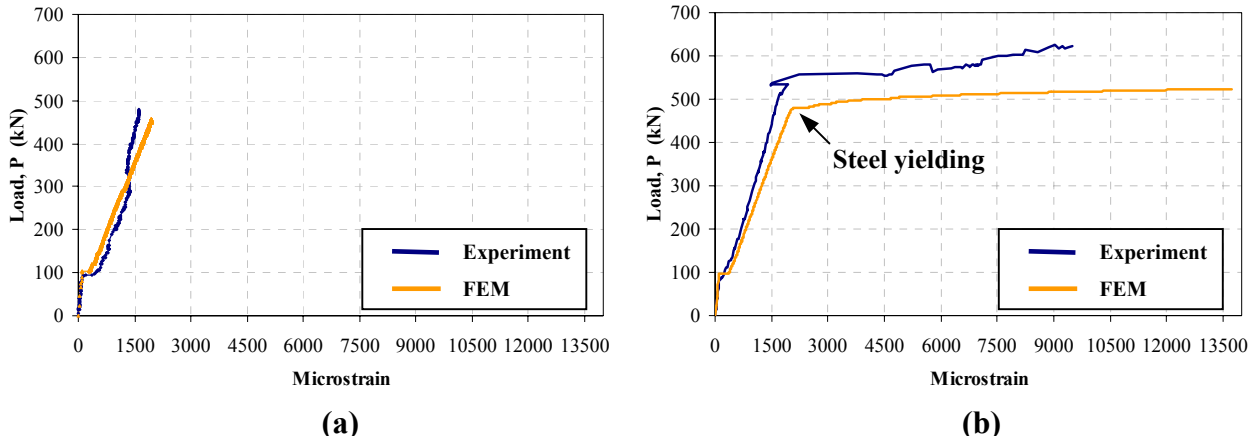


Figure 4.1: Load-Tensile Strain Plot for Main Steel Rebar: (a) Control Beam; (b) Shear-Strengthened Beam

Compressive Strain in Concrete

The load-compressive strain (in concrete) plots collected at midspan at the center of the top face from the experiment are compared with results from the finite element analysis in Figure 4.2. For the control beam, the load-compressive strain plots from the finite element analysis and the experimental data have excellent agreement. For the shear-strengthened beam, the load-strain plots from the finite element and experimental results do not correlate well. As shown in the figure, the experimental beam shows unexpected nonlinear behavior for applied loads from 0 to 470 kN. Either erroneous test data or local material imperfections may be the cause. Cracks occurring at the interfaces between the cement and aggregate due to their differences in elastic modulus, thermal coefficient, and response to change in moisture content when the concrete is hardened could be the source of the local material imperfections. At about 490 kN, large strains occur for the finite element model, whereas at a load of 535 kN similar behavior takes place for the experimental beam. These loads are close to the yielding loads of the steel as shown in Figure 4.1. The yielding of the steel explains the large concrete strains.

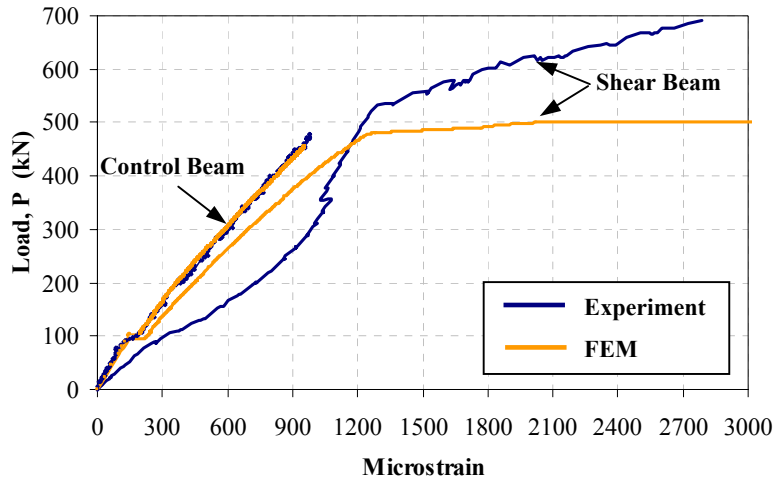


Figure 4.2: Load-Compressive Strain Plot for Concrete

Load-Deflection Plots

Deflections are measured at midspan at the center of the bottom face of the beams. Figure 4.3 shows the load-deflection plots for the control and shear-strengthened beams. In general, the load-deflection plots for the beams from the finite element analyses agree quite well with the experimental data. The finite element load-deflection plots in the linear range are somewhat stiffer than the experimental plots. After first cracking, the stiffness of the finite element models is again higher than that of the experimental beams. There are several effects that may cause the higher stiffnesses in the finite element models. First, microcracks are present in the concrete for the experimental beams, and could be produced by drying shrinkage in the concrete and/or handling of the beams. On the other hand, the finite element models do not include the microcracks. The microcracks reduce the stiffness of the experimental beams. Next, perfect bond between the concrete and steel reinforcing is assumed in the finite element analyses, but the assumption would not be true for the experimental beams. As bond slip occurs, the composite action between the concrete and steel reinforcing is lost. Thus, the overall stiffness of the experimental beams is expected to be lower than for the finite element models (which also generally impose additional constraints on behavior).

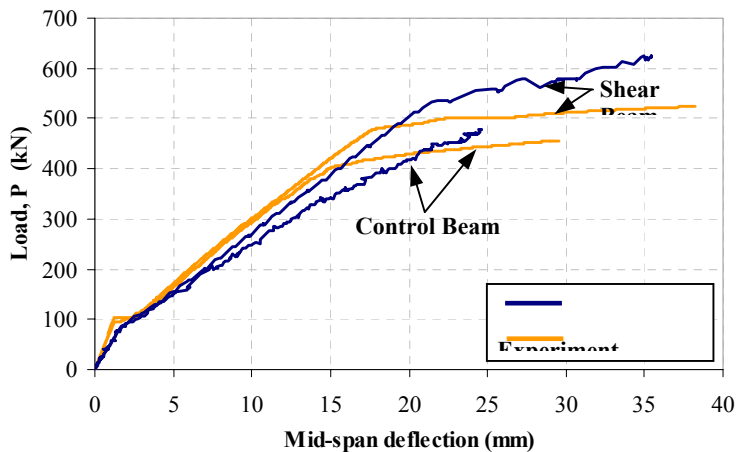


Figure 4.3: Load-Deflection Plot

Loads at Failure

Table 4.1 shows comparisons between the ultimate loads of the experimental beams and the final loads from the finite element models. The final loads for the finite element models are the last applied load steps before the solution diverges due to numerous cracks and large deflections. It is seen that the ANSYS models underestimate the strengths of the beams, as anticipated.

One explanation is that the inclined portions of the steel reinforcement are excluded from the finite element models. Toughening mechanisms at the crack faces [17], i.e. the grain bridging process, interlocking between the cracked faces, crack tips blunted by voids, and the crack branching process, may also slightly extend the failures of the experimental beams before complete collapse. The finite element models do not have these mechanisms. Finally, the material properties assumed in this study may be imperfect.

In the experiment, the failure modes for the beams were as predicted. The control beam failed in shear. The shear-strengthened beam failed in flexure at the midspan, with yielding of the steel reinforcing followed by a compression failure at the top of the beam. Crack patterns obtained from the finite element analyses at the last converged load steps and the failure modes of the experimental beams agree very well. For the finite element model of the control beam, smeared cracks spread over the high shear stress region and occur mostly at the ends of the beam from the support toward the loading area. The finite element program accurately predicts that the control beam fails in shear. For the shear-strengthened beam, numerous cracks occur at midspan rather than underneath the loading location. The crack patterns and steel yielding at the midspan for the finite element shear strengthened beam support the experimental results that the beam fails in flexure.

Table 4.1: Comparisons Between Experimental Ultimate Loads and Finite Element Final Loads

Beam	Ultimate load (kN) from Experiment, Failure Mode*	Final load (kN) from FEA	%Difference
Control beam	475, Shear	455	-5
Shear beam	690, Flexure	525	-24
Percent Gain over Control Beam	45%	15%	

*[14]

Evolutions of Crack Patterns for Concrete

The ANSYS program records a crack pattern at each applied load step. Figure 4.4 shows evolutions of crack patterns developing for each beam. The cracks appear underneath the loading location on the control beam model. For the shear strengthened beam model, there are no compressive cracks underneath the loading location. The appearance of the cracks reflects the failure modes for the beams.

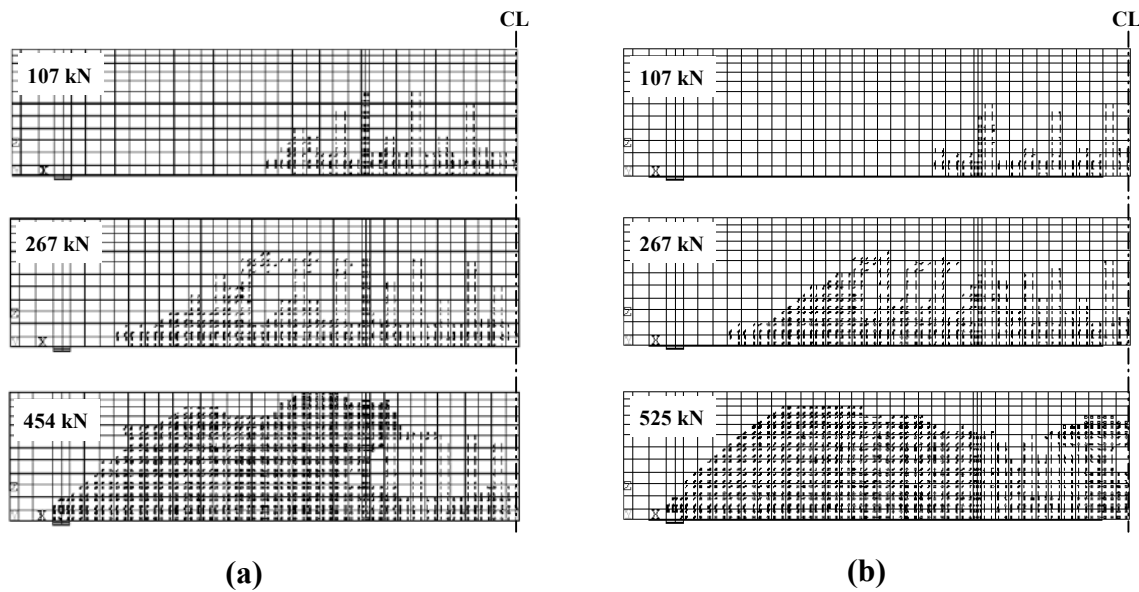


Figure 4.4: Evolution of Crack Patterns: (a) Control Beam; (b) Shear-Strengthened Beam

Conclusions

The general behaviors of the finite element models show good agreement with observations and data from the experimental full-scale beam tests. The addition of GFRP reinforcement to the control beam shifts the behavior of the actual beam and model from a sudden shear failure near the ends of the beam to flexure failure by steel yielding at the midspan. The shear reinforcement increases the load carrying capacity by 45% for the experimental beam and by 15% for the finite element model. This finite element model can be used in additional studies to develop design rules for strengthening reinforced concrete bridge members using FRP.

References

1. ACI 318-99 (1999), American Concrete Institute, Building Code Requirements for Reinforced Concrete, American Concrete Institute, Farmington Hills, Michigan.
2. ACI 440 (2001), American Concrete Institute, Guide for the Design and Construction of Externally Bonded FRP Systems for Strengthening Concrete Structures, American Concrete Institute, Farmington Hills, Michigan.
3. ANSYS (1998) ANSYS User's Manual Revision 5.5, ANSYS, Inc., Canonsburg, PA.
4. Arduini, M., Di Tommaso, A., and Nanni, A., (1997) "Brittle Failure in FRP Plate and Sheet Bonded Beams," *ACI Structural Journal*, 94(4), pp. 363-370.
5. Bangash, M. Y. H. (1989) *Concrete and Concrete Structures: Numerical Modeling and Applications*, Elsevier Science Publishers Ltd., London, England.
6. Chansawat, K., (2000) "Nonlinear Finite Element Analysis of Reinforced Concrete Structures Strengthened With FRP Laminates," personal communication, Corvallis, Oregon..

7. Desayi, P. and Krishnan, S., (1964) "Equation for the Stress-Strain Curve of Concrete," *Journal of the American Concrete Inst.*, 61, pp. 345-350.
8. Hemmaty, Y., (1998) "Modelling of the Shear Force Transferred Between Cracks in Reinforced and Fibre Reinforced Concrete Structures," *Proceedings of the ANSYS Conference*, Vol. 1, Pittsburgh, Pennsylvania.
9. Huyse, L., Hemmaty, Y., and Vandewalle, L., (1994) "Finite Element Modeling of Fiber Reinforced Concrete Beams," *Proceedings of the ANSYS Conference*, Vol. 2, Pittsburgh, Pennsylvania.
10. Kachlakev, D. I., (1998) "Strengthening Bridges Using Composite Materials," *FHWA Report No. OR-RD-98-08*, Corvallis, Oregon.
11. Kachlakev, D.I. and McCurry, D., Jr., (2000) "Simulated Full Scale Testing of Reinforced Concrete Beams Strengthened with FRP Composites: Experimental Results and Design Model Verification," *United States Department of Transportation, Federal Highway Administration*.
12. Kachlakev, D. I., Miller, T. H., Yim, S., Chansawat, K., and Potisuk, T., (2000) "Linear and Nonlinear Finite Element Modeling of Reinforced Concrete Structures Strengthened With FRP Laminates," *United States Department of Transportation, Federal Highway Administration*.
13. Marshall, O. S. and Busel, J. P., (1996) "Composite Repair/Upgrade of Concrete Structures," 4th Materials Conference, "Materials for the New Millennium", editor K. Chong, American Society of Civil Engineers, Washington, D. C.
14. McCurry, D., Jr. and Kachlakev, D. I., (2000) "Strengthening of Full Sized Reinforced Concrete Beam Using FRP Laminates and Monitoring with Fiber Optic Strain Gauges," in "Innovative Systems for Seismic Repair and Rehabilitation of Structures," *Design and Applications*, Technomic Publishing Co., Inc., Philadelphia.
15. Potisuk, T., (2000) "Finite Element Modeling of Reinforced Concrete Beams Externally Strengthened by FRP Composites," *MS Thesis, Oregon State University, Corvallis, Oregon*.
16. Rashid, Y. R., (1968) "Ultimate Strength Analysis of Prestressed Concrete Pressure Vessels," *Nuclear Engineering and Design*, 7(4), pp. 334-344, Amsterdam, Netherlands.
17. Shah, S. P., Swartz, S. E., and Ouyang, C., (1995) *Fracture Mechanics of Concrete*, John Wiley & Sons, Inc., New York, New York.
18. Steiner, W., "Strengthening of Structures with CFRP Strips, (1996) "Advanced Composite Materials for Bridges and Structures, 2nd International Conference, *Proceedings*, editor M.El-Bardry, Montreal, Canada.
19. Suidan, M. and Schnobrich, W. C., (1973) "Finite Element Analysis of Reinforced Concrete," *Journal of the Structural Division, ASCE*, ST10, pp. 2109-2122.
20. Tedesco, J. W., Stallings J. M., and El-Mihilmy, M., (1999) "Finite Element Method Analysis of a Concrete Bridge Repaired with Fiber Reinforced Plastic Laminates," *Computers and Structures*, 72, 379-407.
21. Tedesco, J. W., Stallings J. M., El-Mihilmy, M., and McCauley, M., (1996) "Rehabilitation of Concrete Bridges Using FRP Laminates," 4th Materials Conference, "Materials for the New Millennium", editor K. Chong, American Society of Civil Engineers, Washington, D. C.
22. William, K. J. and Warnke, E. P., (1975) "Constitutive Model for the Triaxial Behavior of Concrete," *Proceedings, International Association for Bridge and Structural Engineering*, Vol. 19, ISMES, Bergamo, Italy, pp. 174.